

## OPTIMIZATION OF 3D PRINTING PARAMETERS FOR PLA/PCL FILAMENT USING THE TAGUCHI METHOD: EFFECTS ON MECHANICAL PROPERTIES AND SHAPE MEMORY PERFORMANCE

<sup>1,\*</sup>Meltem ERYILDIZ , <sup>2</sup>Bekir Kağan KUTLUHAN , <sup>3</sup>Mihrigül EKŞİ ALTAN 

<sup>1,2</sup> Istanbul Beykent University, Mechanical Engineering Department, Istanbul, TÜRKİYE

<sup>3</sup> Yildiz Technical University, Mechanical Engineering Department, Istanbul, TÜRKİYE

<sup>1</sup>[meltemeryildiz@beykent.edu.tr](mailto:meltemeryildiz@beykent.edu.tr), <sup>2</sup>[2003040039@student.beykent.edu.tr](mailto:2003040039@student.beykent.edu.tr), <sup>3</sup>[meksi@yildiz.edu.tr](mailto:meksi@yildiz.edu.tr)

### Highlights

- Taguchi method optimized 3D printing parameters for PLA/PCL blends.
- Lines infill pattern achieved 83% shape recovery rate at 185°C, 40 mm/s.
- Print speed of 40 mm/s and 185°C optimized mechanical and shape memory performance.
- Regression and ANOVA validated effects on mechanical and shape memory properties.

### Graphical Abstract (Optional)



Flowchart of the proposed method



## OPTIMIZATION OF 3D PRINTING PARAMETERS FOR PLA/PCL FILAMENT USING THE TAGUCHI METHOD: EFFECTS ON MECHANICAL PROPERTIES AND SHAPE MEMORY PERFORMANCE

<sup>1,\*</sup> Meltem ERYILDIZ , <sup>2</sup> Bekir Kağan KUTLUHAN , <sup>3</sup> Mihrigül EKŞİ ALTAN 

<sup>1,2</sup> Istanbul Beykent University, Mechanical Engineering Department, Istanbul, TÜRKİYE

<sup>3</sup> Yıldız Technical University, Mechanical Engineering Department, Istanbul, TÜRKİYE

<sup>1</sup>[meltemeryildiz@beykent.edu.tr](mailto:meltemeryildiz@beykent.edu.tr), <sup>2</sup>[2003040039@student.beykent.edu.tr](mailto:2003040039@student.beykent.edu.tr), <sup>3</sup>[meksi@yildiz.edu.tr](mailto:meksi@yildiz.edu.tr)

(Received: 24.01.2025; Accepted in Revised Form: 06.03.2025)

**ABSTRACT:** This study investigates the optimization of 3D printing process parameters for PLA/PCL filament using the Taguchi method. A Taguchi L9 orthogonal array design was employed to explore the effects of print speed (40, 60, 80 mm/s), temperature (185,190,200°C), and infill pattern (the Lines, Gyroid, Triangle) on both mechanical and shape memory properties of the printed parts. The experiments were conducted using a Fused Deposition Modeling (FDM) 3D printer. The mechanical properties, including tensile strength, and shape memory properties such as shape recovery ratio, were evaluated for each combination of process parameters. The experiments revealed that a print speed of 40 mm/s, a nozzle temperature of 185°C, and the Lines infill pattern produced the best shape memory performance, achieving the shape recovery rate of 78.60% and the recovery time of 69 seconds. For tensile strength, the optimal conditions were found to be 40 mm/s, 185°C, and the Gyroid infill pattern, resulting in the highest tensile strength of 21.985 MPa. However, for simplicity and faster production, the Lines infill pattern is preferred. This research provides valuable insights for optimizing the 3D printing process of PLA/PCL filament and enhancing its mechanical and shape memory performance, which is crucial for various applications in biomedical, textile, and packaging industries.

**Keywords:** 3D Printing, Mechanical Properties, PLA/PCL Filament, Shape Memory Properties, Taguchi Method

### 1. INTRODUCTION

Additive manufacturing, commonly known as 3D printing, produces three-dimensional objects by layering material step by step, following a digital design. The advent of 3D printing technology has revolutionized various industries, particularly in the medical field, where it enables the production of patient-specific models, prosthetics, and implants with unparalleled precision and customization. This cutting-edge technology offers the ability to create complex geometries tailored to individual patient needs, enhancing surgical planning and improving overall healthcare outcomes [1].

Of the many materials utilized in 3D printing, Polylactic Acid (PLA) and Polycaprolactone (PCL) have garnered significant attention due to their biodegradability, biocompatibility, and simplicity of processing. PLA, a thermoplastic derived from renewable resources such as corn starch, is widely appreciated for its mechanical properties and environmental friendliness, and it is commonly applied in biomedical fields because of its biodegradability, biocompatibility, and ability to support tissue regeneration and drug delivery systems [2]. PCL, similarly, is a biodegradable polyester known for its reduced melting point, high flexibility, and biocompatibility, making it suitable for various medical and industrial applications [3]. A key drawback of PLA is its brittleness and limited impact resistance, which may limit its application in certain functional parts. Combining PLA with PCL is a good option to overcome these limitations, as PCL's flexibility and low melting point enhance the toughness and durability of the resulting material [4].

Fused deposition modeling (FDM) is an additive manufacturing technique commonly employed to produce geometrically intricate prototypes and components. FDM works by melting thermoplastic filament and forcing it through a heated nozzle layer by layer onto a build platform, where each layer

\*Corresponding Author: Meltem ERYILDIZ, [meltemeryildiz@beykent.edu.tr](mailto:meltemeryildiz@beykent.edu.tr)

solidifies to form a three-dimensional object [5]. While it reduces cycle time and eliminates the need for expensive tools.

Optimizing FDM 3D printing parameters for PLA/PCL material is crucial for achieving high-quality prints with precise dimensions, superior surface finish, and desired mechanical properties, ensuring efficiency and reliability in additive manufacturing processes. The Taguchi method has been widely applied in various fields, including 3D printing and electrospinning, to optimize process parameters and enhance material properties. By employing a systematic design of experiments (DOE) approach, the Taguchi method enables efficient parameter selection while minimizing experimental effort. Hasdiansah et al. [7] optimized FDM 3D printing parameters for TPU using the Taguchi method, identifying layer thickness as the most significant factor affecting surface roughness. Singh et al. [8] optimized FDM 3D printing parameters for PLA-nanographene composites using the Taguchi method, identifying composition as the most significant factor influencing wear resistance. Meyva-Zeybek et al. [9] applied the Taguchi method to optimize electrospinning parameters for PLA and PLA/POSS nanofibers, demonstrating that using a Taguchi L9 orthogonal array significantly reduced the number of experiments while effectively determining the optimal conditions. Nazir et al. [10] applied the Taguchi method to optimize PA-6 nanofiber electrospinning, identifying polymer concentration as the key factor influencing fiber diameter and determining optimal conditions for minimal diameter and variation.

Process parameters like nozzle temperature, print speed, infill pattern, infill density, and layer height influence the final product's dimensional precision, surface quality, and mechanical strength [10]. However, the interplay between these parameters is complex, necessitating a systematic approach to identify the optimal settings. Researchers have extensively investigated the impact of these parameters on part characteristics and explored process parameter optimization, focusing primarily on neat thermoplastic polymers such as PLA, PCL, or ABS. Mohamed et al. [11] examined how factors such as raster angle, layer thickness, build orientation, air gap, road width, and number of contours affect material consumption, build time, and dynamic flexural modulus in FDM. Vidakis et al. [12] explored how six essential 3D printing parameters influence key quality metrics such as surface finish, dimensional precision, and porosity in material extrusion (MEX) additive manufacturing, utilizing robust experimental methods and predictive regression models to optimize part quality and performance. Le et al. [13] studied the optimization of mechanical properties and print time for PLA using FDM, emphasizing the balance between print speed and ultimate strength by varying parameters such as number of outer shells, nozzle diameter, nozzle temperature, infill pattern and infill density through DOE and ANOVA. Despite significant progress, further research in this field remains essential, particularly as each newly developed material in additive manufacturing requires tailored process parameters to optimize its performance characteristics. Understanding how key FDM parameters influence the shape recovery rate is crucial for advancing the practical applications of shape memory materials. Liu et al. [14] focused primarily on investigating the thermoresponsive shape memory effects and material characteristics of PLA/PCL blends, rather than conducting an in-depth study of the FDM process conditions. Qui et al. [15] aimed to produce a PLA/PCL filament, investigating the influence of PCL content on filament geometry, dimensions, surface roughness, and ultimate tensile strength. However, they did not extensively study specific FDM process parameters in their research.

Shape memory properties are also crucial aspects to optimize, as they significantly influence the functionality and responsiveness of the printed structures. Saptaji et al. [16] investigated the activation and shape recovery properties of 3D printed PLA samples, examining the effects of various printing parameters such as thickness, infill density, printing speed, deformation temperature, and recovery temperature, with results showing that the highest recovery ratio of 0.784 was achieved under specific conditions, and the thickness parameter was identified as the most significant factor influencing shape memory behavior. Hosseinzadeh et al. [17] examined the impact of deformation temperature, recovery temperature, and heating rate on the shape recovery of PLA, finding that the optimal conditions (deformation temperature of 53.31°C, recovery temperature of 59.94°C, and heating rate of 8.05°C/min) improved shape recovery from 93.03% to 98.14% in 3D-printed rounded rectangle structures, and

enhanced recovery in diamond and honeycomb structures as well. Eryildiz [18] investigated the effects of 4D printing process parameters, including sample thickness, nozzle temperature, deformation temperature, and holding time, on the shape recovery of PLA, finding that sample thickness had the greatest impact and that increasing deformation, holding, and nozzle temperatures enhanced shape recovery, while greater sample thickness negatively affected it. While various studies have explored the effects of different process parameters on shape memory and recovery of PLA in 4D printing, further research is needed to optimize process parameters for various geometries and applications to enhance the functionality and performance of 4D printed PLA/PCL structures.

In this study, the objective is to optimize the 3D printing process parameters for PLA/PCL filament using the Taguchi method. The Taguchi method, a robust statistical tool for optimizing process parameters, offers an efficient approach to address this challenge. By employing a designed set of experiments, the Taguchi method helps in understanding how various factors impact the quality of 3D-printed objects. This method not only simplifies the optimization process but also enhances the reproducibility and reliability of the results [19]. By systematically analyzing the effects of key parameters, we seek to identify the optimal conditions that yield high-quality prints with improved mechanical properties and shape memory characteristics. Additionally, statistical analyses, including ANOVA and regression modeling, were employed to validate the influence of the selected process parameters on the observed properties. This research will contribute to the growing body of knowledge in the field of additive manufacturing, especially in medical and 4D printing applications, enriching our understanding and capabilities in these cutting-edge fields.

## 2. MATERIAL AND METHODS

### 2.1. Materials

PLA (Natureworks Ingeo® 4043D from Resinex, Turkey), exhibits a melt flow index (MFI) of 6 g/10 min (at 210°C, 2.16 kg), a density of 1.24 g/cm<sup>3</sup>, and a melting point ranging from 145 to 160 °C. PCL, obtained as Perstorp Capa 6500 pellets from Biesterfeld, Turkey has a melt flow index (MFI) of 5.9–7.9 g/10 min (measured at 160°C with a 2.16 kg load), a density of 1.1 g/cm<sup>3</sup>, and a melting point range of 58–60°C. Both PLA and PCL pellets were dried at 40°C for 24 hours in a NÜVE MF 106 oven prior to melt-blending.

### 2.2. Fabrication of PLA/PCL Filament

The PLA/PCL blend (80:20 ratio by weight) was processed using a twin-screw extruder (Rondol, England, L/D=10) at 60 rpm, with the temperature profile from die to feeder set at 150°C, 185°C, 175°C, 165°C, and 80°C. Post-extrusion, the blend was pelletized and dried overnight at 40°C in a NÜVE MF 106 oven. 1.75 mm diameter filament was extruded using a Filament Maker-Composer 350 (3devo, Turkey) at temperatures between 150°C to 170°C, ensuring a filament thickness deviation of only 5 µm.

### 2.3. 3D Printing Process

The blended PLA/PCL filament was loaded into a desktop FDM 3D printer (Flashforge Creator 3 Pro, Turkey) to produce the samples. The printer parameters, such as layer height, bed temperature, infill density, and cooling fan speed, were chosen based on established literature and are listed as fixed parameters in Table 1 [14-15].

**Table 1.** 3D printing parameters for sample fabrication

<b>Printing Parameters</b>	<b>Settings</b>
Nozzle diameter	0.4 mm
Bed temperature	50°C
Layer thickness	0.18 mm
Infill density	60%
Number of shells	3
Top and bottom layers	0
Wall thickness	1.2 mm

Optimization of print speed, nozzle temperature, and infill pattern was conducted using a Taguchi experimental design to enhance mechanical and shape memory properties. Print speed, nozzle temperature, and infill pattern are critical parameters in FDM 3D printing that directly influence mechanical characteristics and shape memory performance of printed parts. Optimizing these parameters ensures that the prints achieve desired levels of strength, dimensional accuracy, and shape retention, crucial for applications in fields such as medicine and advanced manufacturing [20]. Infill patterns are critical for shaping the mechanical properties and shape recovery capabilities in 4D printing. The specific arrangement and geometry of infill patterns within printed parts directly influence factors such as structural strength, flexibility, and the ability to achieve desired shape transformations. Optimizing infill patterns ensures that 4D-printed objects exhibit reliable performance and functionality tailored to their intended applications [21]. The temperature of the nozzle greatly affects both the process and mechanical properties of printed objects. It dictates the material flow dynamics and layer adhesion during deposition, crucial for ensuring structural integrity and dimensional accuracy. Moreover, temperature settings play a pivotal role in activating shape memory effects in responsive materials, enabling the printed parts to undergo programmable transformations over time. Thus, optimizing nozzle temperature is essential for achieving robust mechanical properties and reliable shape-changing capabilities in 4D-printed components [22]. Printing speed is also a critical parameter that impacts both the mechanical properties of the printed objects and the efficiency of the printing process. Optimizing print speed ensures precise deposition of material layers, which is crucial for maintaining dimensional accuracy and structural integrity. Moreover, the rate at which material is deposited influences the bonding between layers, affecting the overall strength, durability, and surface finish of the printed parts. Print speed influences shape recovery in 4D printing by affecting the material's cooling rate and layer adhesion, crucial for controlling the activation and efficacy of shape memory properties [23].

The print speed, nozzle temperature, and infill patterns were selected based on a combination of established literature, preliminary trials, and the technical limitations of the FDM printer used in this study. The print speed range of 40, 60, and 80 mm/s was chosen to explore low, medium, and high-speed settings, balancing the effects on mechanical and shape memory properties while avoiding excessively low speeds that increase print times or high speeds that compromise interlayer adhesion. Similarly, the nozzle temperature range of 185°C, 190°C, and 200°C was determined based on the thermal behavior of PLA and PCL, ensuring optimal material flow and interlayer bonding without thermal degradation or insufficient bonding. The selected infill patterns—Lines, Gyroid, and Triangle—were included to study their distinct mechanical and structural characteristics. Lines were chosen for simplicity and efficiency, Gyroid for isotropic mechanical properties, and Triangle for its rigidity, allowing for a comprehensive analysis of their effects on the mechanical and shape memory behavior of the PLA/PCL blends.

#### 2.4. Characterization

Mechanical characteristics like tensile strength and elongation at break, were evaluated using standard ASTM methods. Tensile tests on the 3D-printed samples were conducted using a Zwick Roell 8497 tensile testing machine equipped with a 20 kN load cell at room temperature, with a crosshead speed of 5 mm/min. Samples were shaped in a dog bone configuration following ASTM D638 Type IV

specifications (Figure 1).

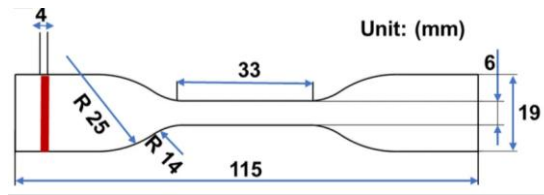


**Figure 1.** Tensile test specimen conforming to ASTM D638 Type IV standards

Differential scanning calorimetry (DSC) was employed with a Perkin Elmer DSC6000 device in a nitrogen atmosphere at a rate of 10°C/min to characterize the melting behavior of the PLA/PCL material. The glass transition temperature of the material was determined for conducting shape memory tests. The shape recovery characteristics of samples printed with FDM were analyzed by programming a temporary shape: heating the sample beyond its glass transition temperature ( $T_g$ ) to set the temporary shape, cooling it below  $T_g$  to fix this shape with a constraint, releasing the constraint upon cooling to allow temporary shape recovery, and heating above  $T_g$  to return to the permanent shape, maintaining stability until reprogramming [18].

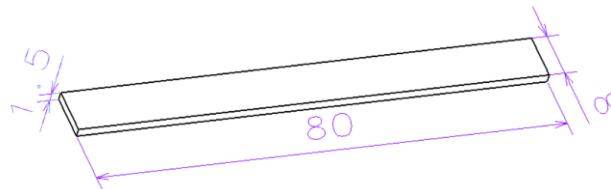


**Figure 2.** Shape memory sample dimensions (units in mm)

During the programming step, shape recovery samples (Figure 2) were exposed to heat in a water bath at the glass transition temperature. The samples were then bent to 90° ( $\theta_u$ ) and held in place for a specified duration. After cooling to 25°C, the external force was removed, allowing the specimen to deform freely due to internal stress ( $\theta_f$ ). Upon reheating to  $T_g$ , the recovery angle  $\theta_r$  was recorded (Figure 3). The shape recovery ratio ( $R_r$ ) was determined using Equation (1) [24]:

$$R_r (\%) = [(\theta_f - \theta_r) / \theta_f] \times 100 \tag{1}$$

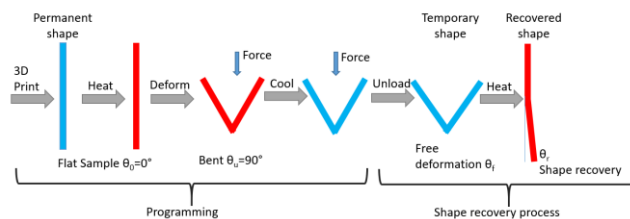


**Figure 3.** The sequential steps of shape-memory-based 4D printing.



**Figure 4.** Experimental setup and workflow of the study

Figure 4 provides a comprehensive visual representation of the experimental procedures and applications conducted in this study.

**2.5. Methodology**

In this experimental study, the Taguchi method using Minitab R16 software was utilized, incorporating print speed, nozzle temperature, and infill pattern as control factors, while tensile strength and shape recovery rate were chosen as the response variables. Each factor was tested at three levels, as specified in Table 2, and the experimental design was structured using an L9 factorial design as depicted in Table 3. Additionally, statistical analyses including ANOVA, regression modeling, and probability plots were performed to evaluate the significance and influence of the selected parameters on the observed mechanical and shape memory properties, ensuring a comprehensive understanding of the process optimization.

**Table 2.** Control factor levels.

Symbol	Control Factor	Level 1	Level 2	Level 3
A	Print Speed (mm/s)	40	60	80
B	Nozzle Temperature (°C)	185	190	200
C	Infill Pattern	Lines	Gyroid	Triangle

The 'larger is better' criterion was used in the Taguchi method to identify optimal process conditions aimed at achieving the highest tensile strength and shape recovery ratio.

**Table 3.** L9 Orthogonal Array Used in the Experimental Study.

No	Print Speed (mm/s) (A)	Nozzle Temperature (°C) (B)	Infill Pattern (C)
1	40	185	Lines
2	40	190	Gyroid
3	40	200	Triangle
4	60	185	Gyroid
5	60	190	Triangle
6	60	200	Lines
7	80	185	Triangle
8	80	190	Lines
9	80	200	Gyroid

### 3. RESULTS AND DISCUSSION

#### 3.1. Thermal Behavior of PLA/PCL Blend

Figure 5 displays the differential scanning calorimetry (DSC) results for the PLA/PCL blend, showing values for the glass transition temperature ( $T_g$ ), cold crystallization temperature ( $T_c$ ), melting temperature ( $T_m$ ), and melting enthalpy ( $\Delta H_m$ ) as 46.57°C, 122.90°C, 150.67°C, and 66.519 J/g, respectively.

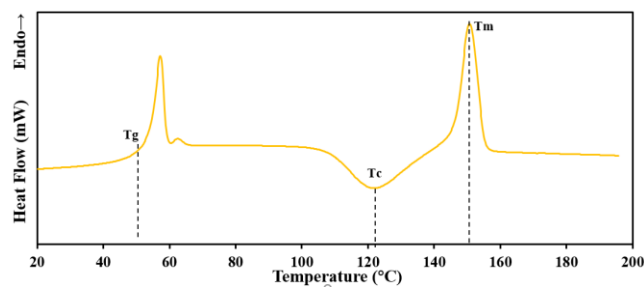


**Figure 5.** Second heating DSC thermogram for the PLA/PCL filament

The glass transition temperature ( $T_g$ ) of neat PLA was 48.40°C, which decreased to 46.57°C with the addition of 20% PCL by weight resulting in improved flexibility and altered thermal characteristics of the PLA/PCL blend [25-26]. In 4D printing processes,  $T_g$  is critical as it affects molecular stability under deformation conditions [18]. The  $T_g$  derived from DSC data was determined to guide shape recovery and deformation temperatures.

#### 3.2. Analysis of Mean

The Taguchi method is a reliable statistical approach for optimizing process parameters to achieve the best possible performance with minimal variability. This method employs an orthogonal array to systematically vary the levels of each factor and evaluate their effects on the desired outcomes [27]. In this study, the Taguchi L9 factorial design was utilized to optimize the 3D printing parameters for PLA/PCL filament, focusing on print speed, nozzle temperature, and infill pattern. The objective was to enhance the tensile strength of the printed parts, with the optimization process guided by the Signal-to-Noise (SN) ratio using the 'larger is better' criterion. The primary factors investigated were print speed (A), nozzle temperature (B), and infill pattern (C). The tensile stress and shape recover rate measurements for each experimental run are summarized in Table 4.

**Table 4.** Tensile stress and shape recovery rate measurements for each experimental run

No	Print Speed (mm/s) (A)	Nozzle Temperature (°C) (B)	Infill Pattern (C)	Tensile Stress (MPa)	Recovery Rate (%)	Time (s)
1	40	185	Lines	20.596	78.60	69
2	40	190	Gyroid	21.678	58.22	43
3	40	200	Triangle	18.196	79.66	53
4	60	185	Gyroid	21.985	70.56	29
5	60	190	Triangle	17.849	61.07	44
6	60	200	Lines	19.572	83.00	43
7	80	185	Triangle	17.563	73.18	75
8	80	190	Lines	20.429	73.89	100
9	80	200	Gyroid	21.724	55.85	120

The Signal-to-Noise (SN) ratio has an essential role in determining the optimal parameter settings, particularly when applying the 'larger is better' criterion to optimize a response variable, such as tensile strength and shape memory rate. Based on the SN ratios calculated for each experimental run (Figure 6), the optimal parameter combinations were identified as A1B1C2—where A1 corresponds to a print speed of 40 mm/s, B1 to a nozzle temperature of 185°C, and C2 to the Gyroid infill pattern for mechanical test results—and A1B1C1—where C1 is the Lines infill pattern—for shape recovery test results. These combinations yielded the highest SN ratios, indicating the most favorable conditions for maximizing tensile strength and shape recovery.

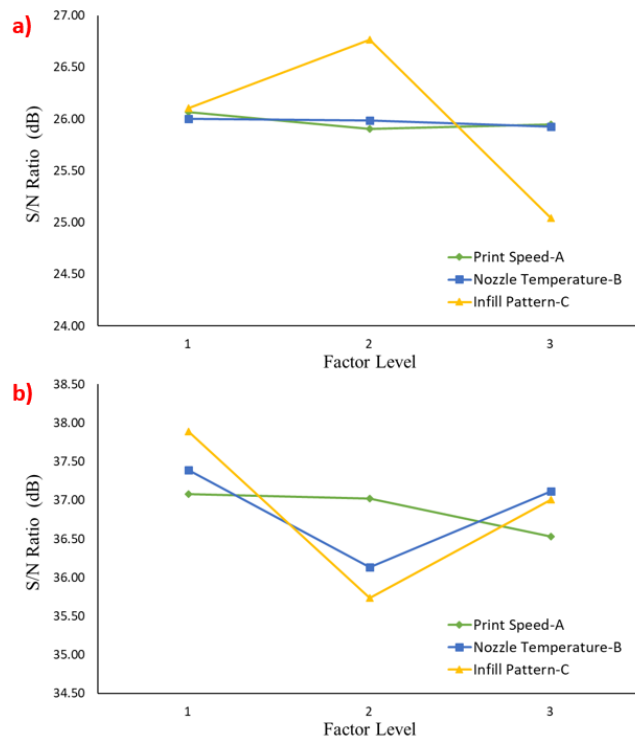


**Figure 6.** SN ratios for a) tensile test, b) shape recovery rate.

### 3.3. Mechanical properties optimization

#### 3.3.1. Impact of print speed on tensile mechanical properties

The print speed did not show a significant effect on the tensile strength of the printed samples. Lower print speeds, particularly at 40 mm/s, generally resulted in higher tensile stress values. For instance, Run 2 (40 mm/s, 190°C, Gyroid) achieved a tensile stress of 21.678 MPa, whereas Run 7 (80 mm/s, 185°C, Triangle) registered 17.563 MPa (Figure 7, Table 4).

A slower print speed allows the extruded filament more time to fuse with the preceding layers, enhancing interlayer adhesion [28]. Enhanced adhesion contributes to improved mechanical properties, as evidenced by the higher tensile stress values. Conversely, higher print speeds can result in inadequate bonding due to rapid deposition, which can lead to weaker mechanical performance [29].

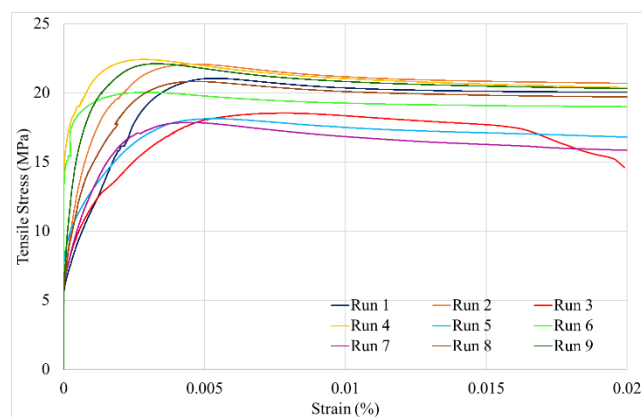


Figure 7. Stress-strain curves of printed PLA/PCL blends for each experimental run.

#### 3.3.2. Impact of Nozzle Temperature on Tensile Mechanical Properties

Nozzle temperature affects the viscosity of the extruded filament, the degree of layer adhesion, and the overall print quality. In this study, nozzle temperature (185°C, 190°C, and 200°C) did not show a significant effect on the tensile strength of the printed PLA/PCL parts.

A lower nozzle temperature of 185°C was identified as optimal for achieving higher tensile strength. This is because at 185°C, the PCL in the blend, which has a lower melting point, is sufficiently melted to enhance flexibility and interlayer adhesion without degrading its structural integrity. This temperature allows the PLA to bond effectively while maintaining the elastic properties provided by the PCL, resulting in superior mechanical performance. For example, at 185°C, combined with a print speed of 60 mm/s and a Gyroid infill pattern, the tensile strength reached 21.985 MPa. This suggests that the balance between PLA's rigidity and PCL's flexibility is best maintained at this temperature, leading to improved tensile properties [30].

At higher temperatures, such as 200°C, the tensile strength decreased. The increased temperature improves the flow and bonding of PLA but may lead to thermal degradation of PCL, reducing the overall mechanical performance of the blend. The study found that higher temperatures tend to weaken the material's mechanical properties, as evidenced by a tensile strength of only 17.849 MPa at 200°C.

#### 3.3.3. Impact of Infill Pattern on Tensile Mechanical Properties

The infill pattern is a vital factor in 3D printing that greatly affects the tensile mechanical properties of the printed parts. Different infill patterns distribute stress and strain differently throughout the printed structure, affecting the overall strength and durability of the part. In this study, three infill patterns—Lines, Gyroid, and Triangle—were analyzed to assess their impact on the tensile strength of PLA/PCL

blends.

The lines infill pattern emerged as one of the most effective for maximizing tensile strength. This pattern, consisting of straight lines oriented at alternating angles in each layer, provides a uniform distribution of stress along the primary loading direction. The simplicity of this pattern reduces print time while ensuring sufficient interlayer bonding. At a print speed of 40 mm/s and a nozzle temperature of 185°C, the Lines pattern achieved a tensile strength of 20.596 MPa, indicating its effectiveness in enhancing mechanical properties without compromising print efficiency. In accordance with our study, Mishra et al. [31] demonstrated that the Lines infill pattern provided maximum mechanical properties, highlighting its effectiveness in enhancing impact resistance and overall structural integrity in 3D-printed components.

The Lines infill pattern is often favored for its simplicity and efficiency. It consists of straight lines printed at alternating angles in each layer. This pattern is not only quick to print but also provides decent mechanical strength, particularly in one direction (usually the direction of the lines). The alternating pattern of the lines helps distribute stress more evenly across the part, enhancing its ability to withstand tensile forces. Compared to more intricate infill patterns like the Gyroid or the Triangle, the Lines infill pattern may not offer multidirectional strength, but in this specific case, it likely provided sufficient strength in the direction where it was most needed, contributing to the highest tensile stress observed. Additionally, the simplicity of the Lines pattern means less print head movement, which can reduce the risk of defects and inconsistencies, further improving print quality [32, 33].

The Gyroid infill pattern, known for its complex 3D structure, provided the highest tensile strength in certain configurations. The continuous, curved surfaces of the Gyroid pattern allow for isotropic stress distribution, reducing stress concentration points and improving overall mechanical performance [34]. For example, when printed at 60 mm/s and 185°C, the Gyroid pattern produced a tensile strength of 21.985 MPa, the highest observed in this study (Figure 7, Table 4). This pattern is particularly beneficial in applications requiring balanced mechanical properties in multiple directions. The best parameter combination to maximize the tensile strength of PLA/PCL 3D-printed parts, as determined by the Taguchi optimization, is a print speed of 40 mm/s, a nozzle temperature of 185°C, and the Gyroid infill pattern. This setup achieved the highest tensile strength, demonstrating optimal conditions for creating strong, durable parts with consistent mechanical properties. Kadhum et al. [35] also found that the Gyroid infill pattern delivered the best mechanical performance, consistent with our findings that it enhances tensile strength and durability. Similarly, Biroş et al. [36] showed that the Gyroid infill patterns excel in mechanical resistance, supporting our results on their effectiveness in enhancing tensile strength.

The Triangle infill pattern, while structurally robust, did not perform as well as the Lines or Gyroid infill patterns in terms of tensile strength. The angular geometry of this pattern can lead to localized stress concentrations, which may contribute to lower mechanical strength under tensile loads, a similar observation made by Jasim et al. [37].

### 3.4. Shape Memory Properties Optimization

#### 3.4.1. Impact of Print Speed on Shape Recovery Rate

The shape recovery rate varied significantly with changes in print speed. Print speed directly affects the material deposition rate and cooling dynamics during the FDM printing process [38]. Based on the Taguchi optimization, the optimal parameter combination (A1B1C1: 40 mm/s, 185°C, Lines pattern) yielded a high shape recovery rate of 78.60%, reinforcing the importance of lower print speeds in achieving better shape recovery performance.

As seen in Table 4 and Figure 8, at 40 mm/s (Runs 1–3), the shape recovery rates varied depending on the infill pattern and nozzle temperature. The highest recovery rate at this speed was 79.66% (Run 3, 200°C, Triangle pattern), while the lowest was 58.22% (Run 2, 190°C, Gyroid pattern). This indicates that lower print speeds generally enhance layer bonding and reduce residual stress, but the influence of other parameters, such as infill pattern and nozzle temperature, remains significant. At a lower print speed, the extruded material has more time to cool and bond properly between layers, leading to stronger interlayer

adhesion and less residual stress within the printed part. This stronger bonding is crucial for the shape memory effect, as it allows the material to store and release elastic energy more efficiently when undergoing shape transformations. Similar observations were reported by Şahin and Mardini [39] who found that interlayer adhesion depends heavily on printing speed and interlayer interval time, which significantly influence the mechanical characteristics of 3D-printed structures. Additionally, Weng et al. [40] observed that printing speed, along with factors such as superplasticizer dosage and curing conditions, plays a crucial role in enhancing bond strength between layers in extrusion-based 3D printing processes, further emphasizing the importance of controlling these parameters to enhance the structural integrity of printed components.

At a moderate print speed of 60 mm/s (Runs 4–6), the highest overall shape recovery rate (83.00%) was achieved in Run 6 (200°C, Lines pattern), likely due to a balanced material consistency, thermal history, and interlayer bonding. Additionally, Run 4 (185°C, Gyroid pattern) recorded the fastest shape recovery time (29 seconds), suggesting that moderate speeds allow for efficient elastic energy storage and rapid shape recovery.

At higher print speeds (80 mm/s, Runs 7–9), recovery times increased, and shape recovery rates generally declined. The lowest shape recovery rate (55.85%) was observed in Run 9 (200°C, Gyroid pattern), while Run 8 (190°C, Lines pattern) achieved 73.89%, maintaining a relatively stable performance. This decline at higher speeds is likely due to insufficient cooling time between layers, weaker interlayer adhesion, and increased porosity, which introduce residual stresses that hinder shape recovery. Yang et al. (2020) have demonstrated that lower print speeds can enhance mechanical properties and shape memory performance because of better layer fusion and reduced thermal gradients in the printed part, supporting the findings in this study [41].

These findings confirm that lower to moderate print speeds (40–60 mm/s) yield better shape recovery performance, while higher speeds (80 mm/s) introduce structural inconsistencies. The Taguchi analysis identified 40 mm/s as the optimal print speed, reinforcing previous studies that highlight the importance of deposition rate in controlling shape memory behavior. Achieving an optimal balance between structural integrity and recovery efficiency requires careful parameter selection, particularly in applications where precise shape recovery is critical.

The shape recovery rate is significantly influenced by print speed, as seen in Table 4, where variations in recovery rates align with changes in deposition speed. The highest recovery rate (83.00%) was observed in Run 6 (60 mm/s, 200°C, Lines pattern), while the lowest (55.85%) occurred in Run 9 (80 mm/s, 200°C, Gyroid pattern). However, a single high recovery rate does not necessarily indicate optimal conditions; instead, the overall trend must be considered. The optimal parameter combination (A1B1C1: 40 mm/s, 185°C, Lines) yielded a high recovery rate (78.60%), reinforcing the importance of lower print speeds in achieving better shape memory performance. At higher print speeds (60 mm/s and 80 mm/s), the rapid deposition reduces cooling time between layers, potentially weakening interlayer adhesion and introducing residual stress, which negatively impacts the material's ability to recover its original shape. In contrast, at lower print speeds (40 mm/s), the extended cooling time promotes stronger bonding and better layer fusion, leading to more efficient shape recovery. These findings align with previous studies that highlight the critical role of deposition rate in shape memory behavior, emphasizing that moderate print speeds offer the best balance between structural integrity and recovery efficiency [39,40].

#### 3.4.2. Impact of Nozzle Temperature on Shape Recovery Rate

As shown in Table 4, nozzle temperature significantly influences the shape recovery rate by affecting material viscosity, interlayer bonding, and internal stress distribution during printing. The Taguchi analysis identifies the optimal parameter combination as A1B1C1 (40 mm/s print speed, 185°C nozzle temperature, and Lines infill pattern), meaning that the highest shape recovery rate is not necessarily achieved in a single run but rather through the optimal balance of all parameters.

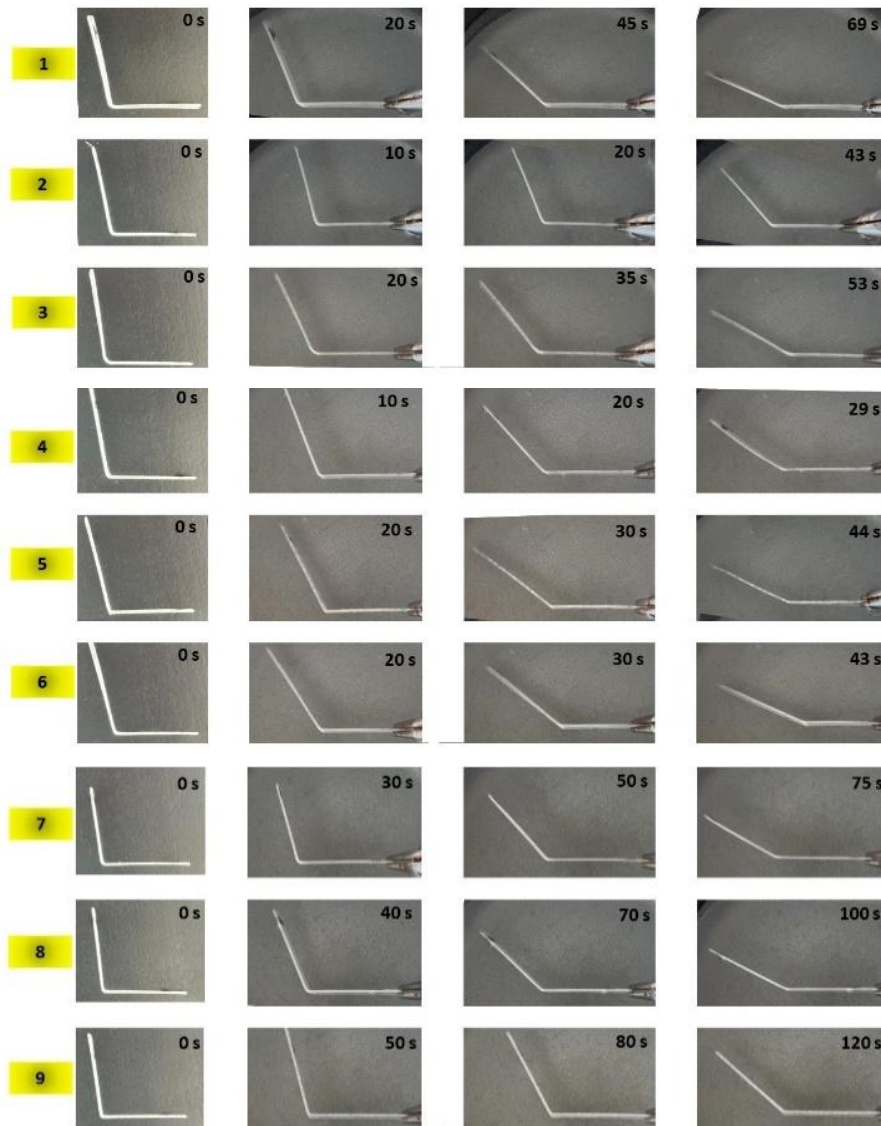


**Figure 8.** Shape recovery rates for all nine experimental runs.

Across the tested conditions, higher nozzle temperatures (200°C) showed inconsistent recovery results, where Run 6 (200°C) exhibited the highest individual recovery rate (83.00%), but Run 9 (200°C) had the lowest (55.85%). This suggests that while increased temperature can improve layer bonding and polymer chain mobility, it may also lead to thermal degradation or excessive fluidity at higher speeds, reducing overall recovery performance. The inconsistency in shape recovery rate at 200°C can be attributed to the combined effects of polymer chain mobility, thermal degradation, and print speed. At this higher temperature, polymer chains gain increased mobility, which can enhance interlayer diffusion [42] and improve shape recovery, as observed in Run 6 (200°C, 60 mm/s, Lines, 83.00%). However, excessive heat can also lead to thermal degradation, causing polymer chain scission and reducing molecular weight [43], which weakens the material's ability to recover its original shape. This effect is particularly pronounced when combined with high print speeds, as seen in Run 9 (200°C, 80 mm/s, Gyroid, 55.85%), where rapid extrusion may have resulted in poor layer adhesion, internal defects, and increased residual stresses that hindered shape recovery. Additionally, at high temperatures, excessive material fluidity can lead to poor layer deposition and structural inconsistencies, further affecting the recovery performance. The infill pattern also plays a role, as the Lines pattern in Run 6 may have facilitated better thermal distribution, while the Gyroid pattern in Run 9 could have contributed to localized stress

concentrations, reducing recovery efficiency. These findings suggest that while a higher nozzle temperature can improve layer bonding, it must be carefully optimized in conjunction with print speed and infill pattern to prevent excessive softening and degradation, ensuring consistent shape memory performance.

Nozzle temperature is crucial in determining the viscosity of the extruded material and its adhesion between layers during the FDM printing process [44]. At the optimal nozzle temperature of 185°C (Runs 1, 4, and 7), the recovery rates remained relatively stable, with Run 1 (40 mm/s, 185°C, Lines) achieving 78.60% and Run 4 (60 mm/s, 185°C, Gyroid) reaching 70.56%. This indicates that 185°C maintains good molecular integrity and adhesion, supporting efficient shape recovery without excessive softening or degradation. The PLA/PCL blend achieves a balance where the material flow is smooth enough to ensure strong interlayer bonding but not so high that it leads to overheating or thermal degradation [45]. This balance is essential for effective shape recovery, as it allows the material to maintain its integrity and undergo elastic deformation, enabling it to revert to its original form when the temperature exceeds its glass transition point. Issabayeva and Shishkovsky [46] observed similar effects, noting that lower temperatures improved shape recovery of PLA by reducing residual stress.

For 190°C (Runs 2, 5, and 8), recovery rates showed more variability, ranging from 58.22% (Run 2, 40 mm/s, Gyroid) to 73.89% (Run 8, 80 mm/s, Lines). This suggests that 190°C may not always provide consistent benefits for shape memory performance, especially when combined with infill patterns that do not optimize thermal diffusion. At higher nozzle temperatures (200°C), the material may become overly fluid, causing poor layer deposition and potential sagging, which can weaken the part's overall structure. This weakened structure negatively impacts the shape recovery rate, as internal defects and weakened bonds hinder the material's capacity to revert to its initial shape [46-47].

The shape recovery rate and time are influenced by nozzle temperature. At 185°C (Runs 1, 4, and 7), recovery rates remained stable (70.56%–78.60%) with moderate recovery times (29–75 s), indicating optimal viscosity and strong interlayer bonding. At 190°C (Runs 2, 5, and 8), recovery rates varied more (58.22%–73.89%) with longer times in some cases (up to 100 s), likely due to increased fluidity affecting layer adhesion. At 200°C (Runs 3, 6, and 9), results were inconsistent — Run 6 achieved the highest recovery rate (83.00%) in 43 s, while Run 9 had the lowest (55.85%) with the longest recovery time (120 s), suggesting that excessive heat can enhance chain mobility [48] but also lead to thermal degradation or weak structural integrity. These findings highlight 185°C as the most stable temperature, while higher temperatures require careful optimization to avoid excessive softening and prolonged recovery times.

### 3.4.3. Effect of Infill Pattern on The Shape Recovery Rate

The infill pattern plays a crucial role in determining the shape recovery rate, as it influences internal stress distribution, energy storage, and deformation behavior. As seen in Table 4, the Lines, Gyroid, and Triangle patterns exhibited varying recovery performances under different conditions, highlighting the importance of selecting the appropriate infill structure. The infill pattern determines the internal geometry and distribution of material within a printed part, affecting its mechanical properties and shape recovery capabilities [46].

Among the tested patterns, the Lines pattern demonstrated the most consistent and favorable results, particularly in Run 6 (60 mm/s, 200°C, Lines) where the highest individual shape recovery rate of 83.00% was observed. Additionally, Run 1 (40 mm/s, 185°C, Lines) achieved a recovery rate of 78.60%, further supporting the effectiveness of this pattern. The superior performance of the Lines pattern can be attributed to its uniform stress distribution and efficient load transfer, which enhances elastic energy storage and release during shape recovery.

The Lines infill pattern creates a continuous path of material that allows for consistent stress distribution and efficient storage and release of elastic energy. This uniform stress distribution is crucial for effective shape recovery, as it minimizes internal stress concentrations that could hinder the material's capacity to revert to its initial shape. Aloyaydi et al. [49] found similar effects in their study, highlighting that optimized infill strategies contribute to enhanced mechanical performance and shape memory

behavior by ensuring even stress distribution and reducing potential deformation-induced stress concentrations.

More complex patterns like the Gyroid and the Triangle may introduce more variability in internal stress distribution, leading to areas of high stress concentration that can adversely affect shape recovery performance. The study by Liu et al. (2020) indicated that simpler infill patterns, such as the Lines, tend to perform better in shape memory applications due to their predictable internal structure and consistent bonding characteristics [21]. The Gyroid pattern, while known for its excellent mechanical stability, showed more variability in recovery performance. In Run 9 (80 mm/s, 200°C, Gyroid), the lowest recovery rate (55.85%) was recorded, whereas Run 4 (60 mm/s, 185°C, Gyroid) achieved a moderate recovery rate of 70.56%. The reduced performance in certain cases may be due to inconsistent energy storage within the complex, curved structure of the Gyroid pattern, which can lead to localized stress concentrations and hinder full shape recovery. The Triangle pattern exhibited intermediate recovery rates, with Run 3 (40 mm/s, 200°C, Triangle) achieving 79.66%, while Run 5 (60 mm/s, 190°C, Triangle) showed a lower recovery rate of 61.07%. The performance variability suggests that while the Triangle pattern provides good structural support, it may not allow for optimal elastic energy release, affecting the efficiency of shape memory behavior.

The shape recovery time varies significantly across different experimental runs, highlighting the influence of processing parameters on the recovery dynamics of the printed structures. As seen in Table 4, the shortest recovery time was observed in Run 4 (29 seconds, 70.56% recovery rate), while the longest was in Run 9 (120 seconds, 55.85% recovery rate). Generally, shorter recovery times indicate faster energy release and efficient structural recovery, whereas longer times suggest delayed response due to weaker interlayer bonding or internal stresses. The optimal combination (A1B1C1: 40 mm/s, 185°C, Lines) not only yielded a high shape recovery rate but also maintained a moderate recovery time (69 seconds), balancing structural integrity and response efficiency. Notably, longer recovery times in Runs 8 and 9 (100s and 120s, respectively) may be attributed to weaker adhesion or increased internal resistance to shape change, further reinforcing the importance of optimized print parameters for enhanced shape memory performance.

### 3.5. Statistical Analysis

To understand the statistical significance of the selected 3D printing parameters on the mechanical and shape memory properties of the PLA/PCL blends, an Analysis of Variance (ANOVA) was performed. The evaluated parameters included print speed (A), nozzle temperature (B), and infill pattern (C), with tensile strength and shape recovery rate chosen as response variables. The results of the ANOVA are summarized in Table 6 and Table 7.

Regression analysis was also conducted to further understand the influence of print speed, nozzle temperature, and infill pattern on tensile stress and shape recovery rate. The regression models provide a quantitative representation of the contributions of these factors to the observed properties of the PLA/PCL blends.

#### 3.5.1. Tensile Strength

The ANOVA results for tensile strength, presented in Table 6, indicate that the infill pattern (C) was the most significant factor affecting the tensile properties, with a  $p$ -value  $< 0.05$ . This suggests that the geometric arrangement of the infill pattern plays a critical role in determining the mechanical strength of the printed parts. In contrast, print speed (A) and nozzle temperature (B) exhibited less significant effects ( $p > 0.05$ ). The results align with previous studies [50], where infill patterns significantly influenced stress distribution and interlayer adhesion.

**Table 5.** ANOVA results for tensile strength

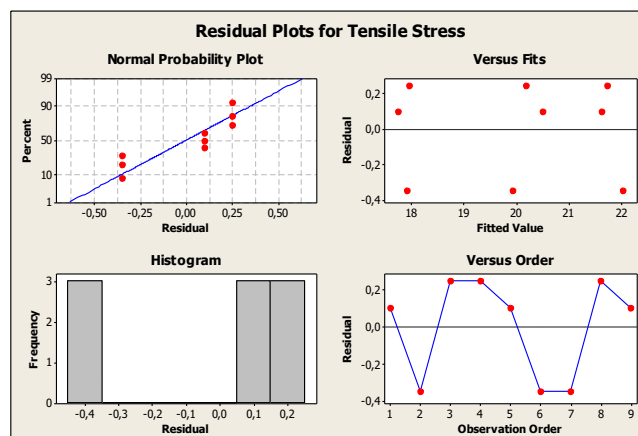
Control factor	DF	Sum of Squares	Mean Square	F-Value	p-value	Contribution (%)
Print speed (mm/s) [A]	2	0.1994	0.0997	0.34	0.746	0.82
Nozzle temperature (°C) [B]	2	0.0751	0.0375	0.13	0.886	0.31
Infill pattern [C]	2	23.3980	11.6990	40.01	0.024	96.45
Error	2	0.5847	0.2924			2.41
Total	8	24.2572				

The relationship between tensile stress and the 3D printing parameters was further explored through regression analysis, as shown in Equation (2):

$$\text{Tensile Stress (MPa)} = 22.8 - 0.126A - 0.109B - 1.16C \quad (2)$$

where A represents print speed, B represents nozzle temperature, and C represents infill pattern.

The regression analysis highlights that the infill pattern (C) exerts the most significant influence on tensile stress, consistent with the ANOVA results where it was found to be statistically significant ( $p < 0.05$ ). The coefficients for print speed (A) and nozzle temperature (B) are smaller, indicating their relatively lower impact on tensile stress within the studied parameter ranges. The coefficient of determination ( $R^2$ ) was found to be 84.6%, indicating that the model explains a substantial portion of the variation in tensile stress. This suggests that the model provides a reasonably good fit for predicting tensile stress based on the selected process parameters. Infill pattern (C) contributes the most (96.45%) to tensile strength, making it the dominant factor, as shown in Table 7. Print speed (A) and nozzle temperature (B) have minimal contributions (0.82% and 0.31%), indicating that they do not significantly influence tensile strength. The error contribution is low (2.41%), meaning the model explains almost all of the variability in the data.

**Figure 9.** The residual plots for tensile stress

The residual plots for tensile stress, as shown in Figure 9, provide a graphical evaluation of the regression model's assumptions and the quality of the fit. The normal probability plot indicates that the residuals follow an approximately linear trend, suggesting that the normality assumption is reasonably satisfied. The residuals versus fitted values plot shows a random scatter with no discernible patterns, indicating that the variance of the residuals is constant and there is no evidence of heteroscedasticity. The histogram of residuals appears symmetric, further supporting the assumption of normality. Lastly, the residuals versus order plot shows no significant trends or patterns, suggesting that the residuals are independent and do not exhibit autocorrelation. These observations confirm that the regression model assumptions are adequately met, and the results can be considered reliable within the tested parameter range.

### 3.5.2. Shape Recovery Rate

The ANOVA analysis for shape recovery (Table 7) indicates that the three studied parameters—print speed, nozzle temperature, and infill pattern—each contribute to variations in the shape recovery rate. Among these, the infill pattern shows a relatively stronger influence, with nozzle temperature also contributing moderately, compared to print speed. While none of the parameters demonstrated a statistically significant effect ( $p > 0.05$ ), their contributions highlight trends that can guide optimization efforts. These results suggest that shape memory performance is influenced by a combination of parameters, and additional factors, such as material composition or layer height, may further enhance optimization strategies for achieving improved recovery rates.

**Table 6.** ANOVA results for shape recovery rate

Control factor	DF	Sum of Squares	Mean Square	F-Value	p-value	Contribution (%)
Print speed (mm/s) [A]	2	36.02	18.01	0.26	0.796	4.63
Nozzle temperature (°C) [B]	2	167.37	83.68	1.19	0.457	21.49
Infill pattern [C]	2	434.53	217.27	3.09	0.245	55.79
Error	2	140.85	70.43			18.09
Total	8	778.78				

The regression equation for shape recovery rate (SRR) is shown in Equation (3):

$$\text{SRR} (\%) = 83.4 - 2.26A - 0.64B - 3.60C \quad (3)$$

where  $A$  represents the print speed in millimeters per second (mm/s),  $B$  represents the nozzle temperature in degrees Celsius (°C), and  $C$  represents the infill pattern used during 3D printing.

The regression analysis indicates that the infill pattern ( $C$ ) has the most noticeable effect on shape recovery rate, as reflected in its coefficient magnitude (-3.60). Print speed ( $A$ ) and nozzle temperature ( $B$ ) also influence the shape recovery rate, but their effects are smaller, as indicated by their respective coefficients of -2.26 and -0.64. The coefficient of determination ( $R^2$ ) was found to be 62.3%, indicating that the model provides a moderate fit for predicting the shape recovery rate based on the selected process parameters. These results indicate that the selected 3D printing parameters have varying impacts on shape memory performance. The infill pattern ( $C$ ) is the most influential factor, contributing 55.79% to shape recovery, followed by nozzle temperature ( $B$ ) with 21.49%, indicating a moderate effect. Print speed ( $A$ ) has a lower impact at 4.63%. The error term accounts for 18.09%, suggesting some variability that may be influenced by additional factors not considered in the model.

The residual plots for shape recovery rate, as presented in Figure 10, offer insights into the adequacy of the regression model. The normal probability plot shows an approximate linear trend, indicating that the residuals are reasonably normally distributed. The residuals versus fitted values plot exhibits a random dispersion, with no evident patterns or systematic bias, suggesting that the assumption of homoscedasticity is met. The histogram of residuals displays a roughly balanced distribution, supporting the normality of residuals. The residuals versus order plot does not show any consistent trends or repetitive patterns, indicating that the residuals are independent over the sequence of observations. These results suggest that the regression model appropriately fits the shape recovery rate data and fulfills the underlying assumptions, providing confidence in the analysis within the tested parameter range.

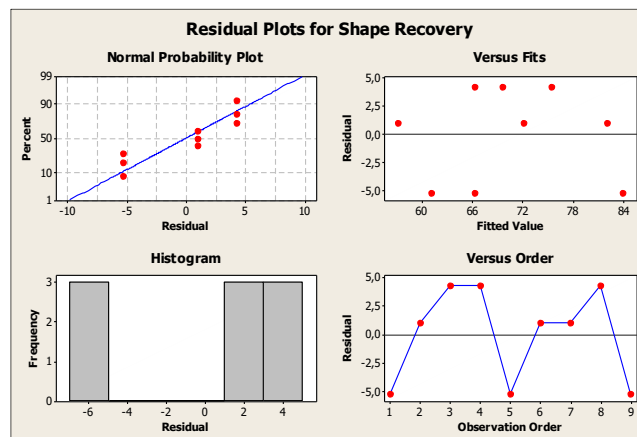


Figure 10. The residual plots for tensile stress

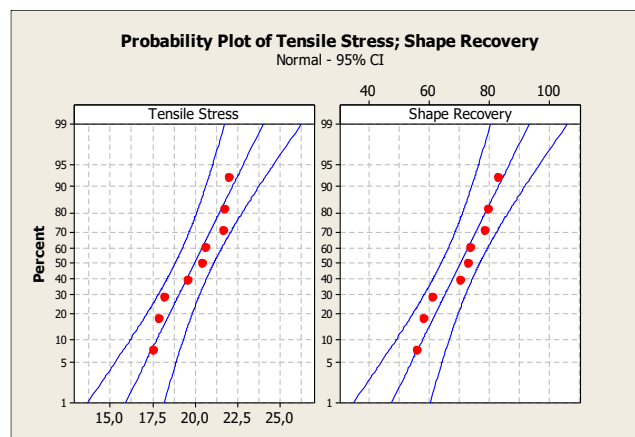


Figure 11. The residual plots for tensile stress and shape recovery ratio

The probability plots for tensile stress and shape recovery, as shown in Figure 11, illustrate how well the data follow a normal distribution. For tensile stress, the mean value is 19.95 MPa with a standard deviation of 1.741 MPa, while for shape recovery, the mean is 70.45% with a standard deviation of 9.866%. The Anderson-Darling (AD) test results for tensile stress ( $AD = 0.408$ ,  $p = 0.272$ ) and shape recovery ( $AD = 0.352$ ,  $p = 0.379$ ) confirm that the residuals for both responses align well with the normal distribution, as the p-values are greater than 0.05. The red data points in both plots fall within the confidence intervals, further validating the assumption of normality. These results suggest that the models for tensile stress and shape recovery are statistically sound, and the residuals do not exhibit significant deviations from normality, supporting the reliability of the analyses.

#### 4. CONCLUSIONS

In this study 3D printing process parameters such as print speed, nozzle temperature, and infill pattern were successfully optimized using the Taguchi method to enhance the mechanical and shape memory properties of PLA/PCL blends printed via Fused Deposition Modeling (FDM). The results indicate that the infill pattern was the most influential factor for tensile strength, while both infill pattern and nozzle temperature had a greater impact on shape recovery rate. In contrast, print speed showed a relatively lower effect on both responses. These findings provide valuable insights for optimizing material performance in applications such as biomedical devices, textiles, and aerospace.

The optimal combination for maximizing shape recovery performance was identified as a print speed of 40 mm/s, a nozzle temperature of 185°C, and a Lines infill pattern. Under these conditions, the shape recovery rate of 78.60% and the recovery time of 69 s were achieved, demonstrating the importance of slower print speeds, optimal thermal control, and simpler infill geometries for enhanced shape memory

capabilities. Conversely, higher nozzle temperatures (190°C and 200°C) and more complex infill patterns, such as the Gyroid, resulted in lower recovery rates and longer recovery times due to weakened interlayer bonding and increased internal stresses.

For mechanical properties, the study revealed that a lower print speed and a nozzle temperature of 185°C, along with a Gyroid infill pattern, resulted in the greatest tensile strength. However, for simplicity and faster production, the Lines infill pattern could be preferred over the Gyroid, as it offers sufficient tensile strength while reducing print time and complexity.

Statistical analysis, including ANOVA and regression modeling, validated the influence of the studied parameters on both tensile strength and shape memory performance. The ANOVA results identified the infill pattern as the most significant factor for tensile strength, while regression analysis quantified the impact of print speed, nozzle temperature, and infill pattern. Residual and probability plots confirmed the reliability of the models, ensuring their accuracy in predicting PLA/PCL blend performance under different 3D printing conditions.

These findings contribute valuable insights into optimizing FDM parameters for PLA/PCL blends, supporting the development of advanced materials for biomedical and 4D printing applications. The Taguchi method proved effective in identifying optimal print parameter combinations, enhancing reproducibility and reliability in process optimization.

### **Declaration of Ethical Standards**

The authors declare to comply with all ethical guidelines, including authorship, citation, data reporting, and original research publication.

### **Credit Authorship Contribution Statement**

All authors made equal contributions to this study.

### **Declaration of Competing Interest**

The authors declare that they have no conflict of interest.

### **Funding / Acknowledgements**

This study was supported by Scientific and Technological Research Council of Turkey (TUBITAK) under the Grant Number 123M748. The authors thank to TUBITAK for their supports.

### **Data Availability**

Data available on request from the authors

### **REFERENCES**

- [1] O. Öztürk, M. A. Şen, and M. Aydın, "The influence of fused filament fabrication parameters on the fracture behavior of PLA specimens considering energy consumption," *Konya Journal of Engineering Sciences*, vol. 12, no. 2, pp. 451–464, 2024.
- [2] S. Solechan, A. Suprihanto, S.A. Widyanto, J. Triyono, D. F. Itriya, J. P. Siregar, and T. Cionita, "Investigating the effect of PCL concentrations on the characterization of PLA polymeric blends for biomaterial applications," *Materials*, vol. 15, no. 20, Art. no. 7396, 2022.
- [3] T. C. Mokhena, M. B. Chabalala, S. Mapukata, A. Mtibe, L. Hlekelele, Z. Cele, and K. Shingange. "Electrospun PCL-based materials for health-care applications: an overview," *Macromolecular Materials and Engineering*, vol. 309, no. 8. Art. no. 2300388, 2024.
- [4] T. Patrício, M. Domingos, A. Gloria, U. D'Amora, J.F. Coelho, and P.J. Bártolo, "Fabrication and

- characterisation of PCL and PCL/PLA scaffolds for tissue engineering," *Rapid Prototyping Journal*, vol. 20, no. 2, pp. 145-156, 2014.
- [5] A. Alafaghani and A. Qattawi, "Investigating the effect of fused deposition modeling processing parameters using Taguchi design of experiment method," *Journal of Manufacturing Processes*, vol. 36, Dec., pp. 164-174, 2018.
- [6] H. Hasdiansah, R. I. Yaqin, P. Pristiansyah, M. L. Umar, and B. H. Priyambodo, "FDM-3D printing parameter optimization using taguchi approach on surface roughness of thermoplastic polyurethane parts," *International Journal on Interactive Design and Manufacturing (IJIDeM)*, vol. 17, no. 6, pp. 3011-3024, 2023.
- [7] S. Singh, R.K. Attri, and S. Trivedi, "Optimization of FDM 3D printing process parameters for improving wear characteristics of PLA-nGr composite using taguchi DOE". *Journal of Materials Engineering and Performance*, Oct., pp. 1-9. 2024.
- [8] Y. Meyva-Zeybek and C. Kaynak, "Electrospinning of PLA and PLA/POSS nanofibers: use of taguchi optimization for process parameters," *Journal of Applied Polymer Science*, vol. 138, no.3, Art. no. 49685, 2021.
- [9] A. Nazir, N. Khenoussi, L. Schacher, T. Hussain, D. Adolphe, and A.H. Hekmati, "Using the taguchi method to investigate the effect of different parameters on mean diameter and variation in PA-6 nanofibres produced by needleless electrospinning," *RSC Advances*, vol. 5, no.94, pp. 76892-76897, 2015.
- [10] A. Dey and N. Yodo, "A systematic survey of FDM process parameter optimization and their influence on part characteristics," *Journal of Manufacturing and Materials Processing*, vol. 3, no. 3, Art. no. 64, 2019.
- [11] O.A. Mohamed, S.H. Masood, and J.L. Bhowmik, "Mathematical modeling and FDM process parameters optimization using response surface methodology based on Q-optimal design," *Applied Mathematical Modelling*, vol. 40, no. 23-24, pp. 10052-10073, 2016.
- [12] N. Vidakis, C. David, M. Petousis, D. Sagris, N. Mountakis, and A. Moutsopoulou, "The effect of six key process control parameters on the surface roughness, dimensional accuracy, and porosity in material extrusion 3D printing of polylactic acid: prediction models and optimization supported by robust design analysis," *Advances in Industrial and Manufacturing Engineering*, vol. 5, Nov., Art. no. 100104, 2022.
- [13] L. Le, M. A. Rabsatt, H. Eisazadeh, and M. Torabizadeh, "Reducing print time while minimizing loss in mechanical properties in consumer FDM parts," *International Journal of Lightweight Materials and Manufacture*, vol. 5, no. 2, pp. 197-212, 2022.
- [14] H. Liu, H. He, and B. Huang, "Favorable thermoresponsive shape memory effects of 3D printed poly (lactic acid)/poly ( $\epsilon$ -caprolactone) blends fabricated by fused deposition modeling". *Macromolecular Materials and Engineering*, vol. 305, no. 11, Art. no. 2000295, 2020.
- [15] H. M. Qiu, K. W. Hou, J. P. Zhou, W. J. Liu, J. B. Wen, and Q. F. Gu, "Preparation of biodegradable PLA/PCL composite filaments: effect of PLA content on strength," *IOP Conference Series: Materials Science and Engineering*, vol. 770, no. 1, Art. no. 012059, 2020.
- [16] K. Saptaji, C. O. Rochmad, O. A. Juniasih, G. K. Sunnardianto, F. Triawan, A. I. Ramadhan, and A. Azhari, "Enhancing shape-recovery ratio of 4D printed polylactic acid (PLA) structures through processing parameter optimization," *Progress in Additive Manufacturing*, vol. 9, no. 6, pp. 1869-1881, 2024.
- [17] M. Hosseinzadeh, M. Ghoreishi, and K. Narooei, "An investigation into the effect of thermal variables on the 3D printed shape memory polymer structures with different geometries," *Journal of Intelligent Material Systems and Structures*, vol. 33, no. 5, pp. 715-726, 2022.
- [18] M. Eryildiz, "Influence of process parameters on the shape recovery properties of 4D-printed polylactic acid parts produced by fused deposition modeling," *Journal of Materials Engineering and Performance*, vol. 32, no. 9, pp. 4258-4269, 2023.
- [19] P. Kumar, P. B. Barua, J. L. Gaindhar, "Quality optimization (multi-characteristics) through

- Taguchi's technique and utility concept," *Quality and Reliability Engineering International*, vol. 16, no. 6, pp. 475-485, 2000.
- [20] D. Syrlybayev, B. Zharylkassyn, A. Seisekulova, M. Akhmetov, A. Perveen, and D. Talamona, "Optimisation of strength properties of FDM printed parts—A critical review," *Polymers*, vol. 13, no. 10, Art. no. 1587, 2021.
- [21] T. Liu, L. Liu, C. Zeng, Y. Liu, and J. Leng, "4D printed anisotropic structures with tailored mechanical behaviors and shape memory effects," *Composites Science and Technology*, vol. 186, Jan., Art. no. 107935, 2020.
- [22] J. Wang, Z. Wang, Z. Song, L. Ren, Q. Liu, and L. Ren, "Programming multistage shape memory and variable recovery force with 4D printing parameters," *Advanced Materials Technologies*, vol. 4, no. 11, Art. no. 1900535, 2019.
- [23] Y. S. Alshebly, and M. Nafea, "Effects of printing parameters on 4D-printed PLA actuators," *Smart Materials and Structures*, vol. 32, no. 6, Art. no. 064008, 2023.
- [24] D. Kong, A. Guo, H. Wu, X. Li, J. Wu, Y. Hu, and S. Guo, "Four-dimensional printing of polymer-derived ceramics with high-resolution, reconfigurability, and shape memory effects," *Additive Manufacturing*, vol. 83, Mar., Art. no. 104050, 2024.
- [25] S. Ma, Z. Jiang, M. Wang, L. Zhang, Y. Liang, Z. Zhang, and L. Ren, "4D printing of PLA/PCL shape memory composites with controllable sequential deformation," *Bio-Design and Manufacturing*, vol. 4, Jul., pp. 867-878, 2021.
- [26] P. Kiani, M. Sedighi, M. Kasaeian-Naeini, and A. H. Jabbari, "High cycle fatigue behavior and thermal properties of PLA/PCL blends produced by fused deposition modeling," *Journal of Polymer Research*, vol. 30, no. 7, Art. no. 264, 2023.
- [27] C. Hamzaçebi, P. Li, P.A.P. Pereira, and H. Navas, "Taguchi method as a robust design tool. Quality Control-Intelligent Manufacturing," in *Quality Control - Intelligent Manufacturing, Robust Design and Charts*, P. Li, P. A. R. Pereira, and H. Navas, Eds. London: IntechOpen, Mar., pp. 1-19, 2020.
- [28] S. H. Ahn, M. Montero, D. Odell, S. Roundy, and P. K. Wright, "Anisotropic material properties of fused deposition modeling ABS," *Rapid prototyping journal*, vol. 8, no. 4, pp. 248-257, 2002.
- [29] M. Domingo-Espin, J. M. Puigoriol-Forcada, A. A. Garcia-Granada, J. Llumà, S. Borros, and G. Reyes, "Mechanical property characterization and simulation of fused deposition modeling polycarbonate parts," *Materials & Design*, vol. 83, Oct., pp. 670-677, 2015.
- [30] A. Li, X. G. Chen, L. Y. Zhang, and Y. F. Zhang, "Temperature and infill density effects on thermal, mechanical and shape memory properties of polylactic acid/poly ( $\epsilon$ -caprolactone) blends for 4d printing," *Materials*, vol. 15, no. 24, Art. No. 8838, 2022.
- [31] P. K. Mishra, P. Senthil, S. Adarsh, M. S. Anoop, "An investigation to study the combined effect of different infill pattern and infill density on the impact strength of 3D printed polylactic acid parts," *Composites Communications*, vol. 24, Apr., Art. No. 100605, 2021.
- [32] T. S. Tamir, G. Xiong, Q. Fang, X. Dong, Z. Shen, and F. Y. Wang, "A feedback-based print quality improving strategy for FDM 3D printing: an optimal design approach," *The International Journal of Advanced Manufacturing Technology*, vol. 120, no. 3, pp. 2777-2791, 2022.
- [33] A. R. Avdeev, A. A. Shvets, and I. S. Torubarov, "Investigation of kinematics of 3D printer print head moving systems," *Proceedings of the 5th International Conference on Industrial Engineering (ICIE 2019)*, vol. 15, Dec., pp. 461-471, 2020.
- [34] G. Chouhan and G. Bala Murali, "Designs, advancements, and applications of three-dimensional printed gyroid structures: A review," *Proceedings of the Institution of Mechanical Engineers, Part E: Journal of Process Mechanical Engineering*, vol. 238, no. 2, pp. 965-987, 2024.
- [35] A. H. Kadhum, S. Al-Zubaidi, and S. S. Abdulkareem, "Effect of the infill patterns on the mechanical and surface characteristics of 3D printing of PLA, PLA+ and PETG materials," *ChemEngineering*, vol. 7, no. 3, Art. no. 46, 2023.
- [36] M. T. Birosz, D. Ledenyak, and M. Ando, "Effect of FDM infill patterns on mechanical properties".

- Polymer Testing*, vol. 113, Sep., Art. no. 107654, 2022.
- [37] M. F. Jasim, T. F. Abbas, and A. F. Huayier, "The effect of infill pattern on tensile strength of PLA material in fused deposition modeling (FDM) process," *Engineering and Technology Journal*, vol. 40, no. 21, pp. 1723-1730, 2022.
- [38] A. Chalgham, A. Ehrmann, I. Wickenkamp, "Mechanical properties of FDM printed PLA parts before and after thermal treatment," *Polymers*, vol. 13, no. 8, Art. no. 1239, 2021.
- [39] H. G. Şahin and A. Mardani, "Mechanical properties, durability performance and interlayer adhesion of 3DPC mixtures: a state-of-the-art review," *Structural Concrete*, vol. 24, no. 4, pp. 5481-5505, 2023.
- [40] Y. Weng, M. Li, D. Zhang, M. Tan, and S. Qian, "Investigation of interlayer adhesion of 3D printable cementitious material from the aspect of printing process," *Cement and Concrete Research*, vol. 143, May., Art. no. 106386, 2021.
- [41] T. Yang and C. Yeh, "Morphology and mechanical properties of 3D printed wood fiber/polylactic acid composite parts using fused deposition modeling (FDM): the effects of printing speed," *Polymers*, vol. 12, no. 6, Art. no. 1334, 2020.
- [42] S. Mani and R. Khare, "Effect of chain flexibility and interlayer interactions on the local dynamics of layered polymer systems," *Macromolecules*, vol. 51, no. 2, pp. 576-588, 2018.
- [43] J. Yoon, H. Jin, I. Chin, C. Kim, and M. Kim, "Theoretical prediction of weight loss and molecular weight during random chain scission degradation of polymers," *Polymer*, vol. 38, no. 14, pp. 3573-3579, 1997.
- [44] Y. Lyu, H. Zhao, X. Wen, L. Lin, A. Schlarb, and X. Shi, "Optimization of 3D printing parameters for high-performance biodegradable materials," *Journal of Applied Polymer Science*, vol. 138, no. 32, Art. no. 50782, 2021.
- [45] K. Elhatab, S. Bhaduri, and P. Sikder, "Influence of fused deposition modelling nozzle temperature on the rheology and mechanical properties of 3D printed  $\beta$ -tricalcium phosphate (TCP)/polylactic acid (PLA) composite," *Polymers*, vol. 14, no. 6, Art. no. 1222, 2022.
- [46] Z. Issabayeva and I. Shishkovsky, "Prediction of the mechanical behavior of polylactic acid parts with shape memory effect fabricated by FDM," *Polymers*, vol. 15, no. 5, Art. no. 1162, 2023.
- [47] M. Barletta, A. Gisario, and M. Mehrpouya, "4D printing of shape memory polylactic acid (PLA) components: investigating the role of the operational parameters in fused deposition modelling (FDM)," *Journal of Manufacturing Processes*, vol. 61, Jan., pp. 473-480, 2021.
- [48] S. J. Zhen, "The effect of chain flexibility and chain mobility on radiation crosslinking of polymers," *Radiation Physics and Chemistry*, vol. 60, no. 4-5, pp. 445-451, 2001.
- [49] B. Aloyaydi, S. Sivasankaran, and A. Mustafa, "Investigation of infill-patterns on mechanical response of 3D printed poly-lactic-acid," *Polymer Testing*, vol. 87, Jul., Art. no. 106557, 2020.
- [50] M. Othmani, K. Zarbane, and A. Chouaf, "Effect of infill and density pattern on the mechanical behaviour of ABS parts manufactured by FDM using Taguchi and ANOVA approach," *Archives of Materials Science and Engineering*, vol. 111, no. 2, pp. 66-77, 2021.